

Resonant Degenerate Four-Wave Mixing in SO₂

W. WEI^{a,b}, Z.Z. LU^{a,c,*}, Q. DONG^c, Y.L. SUN^c, L. MA^c,
J.L. LIAO^c, J.F. LIU^c, X.P. XIE^a AND W. ZHAO^a

^aState Key Laboratory of Transient Optics and Photonics,
Xi'an Institute of Optics and Precision Mechanics (XIOPM),
Chinese Academy of Sciences (CAS), Xi'an 710119, China

^bUniversity of Chinese Academy of Sciences (UCAS), Beijing 100049, China

^cSchool of Physics and Optoelectronic Engineering, Xidian University, Xi'an 710071, China

(Received January 21, 2019; in final form March 6, 2020)

We report an experimental investigation of degenerate four-wave mixing spectrum of SO₂. A novel beam-split technique is used to compensate the beam drift caused by the laser itself and disturbance from the environment. Degenerate four-wave mixing spectra of the transition $B^1B_1 \leftarrow X^1A_{11}$ for SO₂ are obtained. The degenerate four-wave mixing signal intensity as a function of the total input laser energy is measured. The effects of the laser field intensity on the degenerate four-wave mixing spectrum are analyzed. Our results show that the degenerate four-wave mixing signal intensity rises with laser intensity and tends to saturate. Then, a dip begins to appear at resonance in the profile with increase in laser field. The existence of saturation for degenerate four-wave mixing signal intensity and spectrum profile confirms the prediction of previous theoretical work.

DOI: [10.12693/APhysPolA.137.1022](https://doi.org/10.12693/APhysPolA.137.1022)

PACS/topics: 32.70.Jz, 34.50.-s

1. Introduction

Laser techniques are now widely used for the study of combustion and monitoring of pollutant formation. Linear techniques such as absorption spectroscopy and laser-induced fluorescence (LIF) are frequently used [1-3]. LIF allows 2-dimensional imaging and has been successfully applied in engines. Planar laser-induced fluorescence (PLIF) is used to image the flame topography of a turbulent flame [4]. LIF and PLIF have been widely applied [5-7] although interpretation of the signal is often complicated by collisional quenching.

Non-linear techniques offer particular advantages in such situations, owing to the coherent nature of the generated signal [8].

Degenerate four-wave mixing (DFWM) is a non-linear optical process that is widely used for detection of trace species [9-14] and for the measurement of thermodynamic parameters [15, 16]. The physics of the DFWM process has been the subject of numerous theoretical investigations since the late 1970's. These theoretical efforts were reviewed thoroughly by Abrams et al. [17], and Williams et al. [18, 19]. Effects of laser polarization and collisions on DFWM signal generation in the low-intensity or perturbation theory limit were analyzed in great detail. Later, the theory was extended to include saturation effects. Reichardt and Lucht [20] and Dai-Hyuk Yu et al. [21] predicted DFWM saturation effects with increase in laser field intensity.

However, the extremely high demands of the stability of the optical path arrangement limit its scope, and the correctness of theoretical predictions lacks experimental verification. In this paper, a novel compensated beam-split technique is employed to improve the stability of the optical system. An experimental study is carried out to investigate the influence of the laser field on the DFWM spectrum of SO₂. Our results clearly demonstrate that the DFWM technique provides an excellent tool to test the accuracy of line positions, which is mostly limited by the Doppler broadening.

2. The experimental setup

A forward DFWM setup has been used in the present work. As shown in Fig. 1, in the forward geometry all the laser beams are incident from the same side, and are arranged in a three-dimensional box-type geometry. The generated signal beam propagates in the direction that fulfills the phase-matching condition.

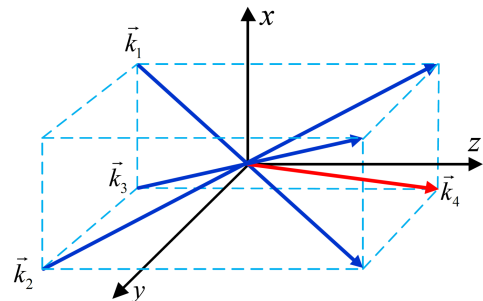


Fig. 1. Phase-matching configurations for DFWM: DFWM with forward geometry.

*corresponding author; e-mail: luhit@126.com

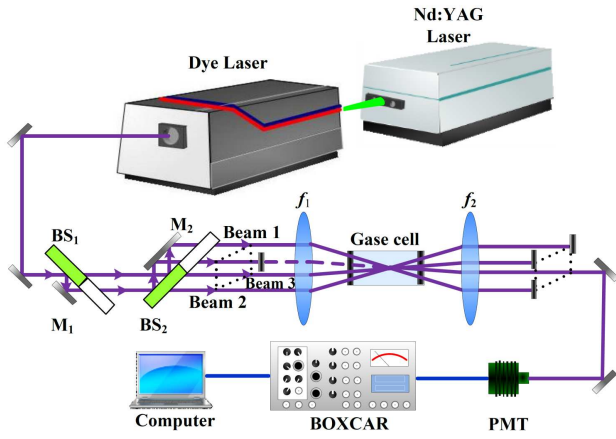


Fig. 2. Experimental setup of DFWM with forward geometry for the SO_2 .

The experimental setup for the DFWM measurements is presented in Fig. 2. A chamber is filled with SO_2 . A dye laser (ScanmatePro, LAMBDA PHYSIK) is used to generate a laser output (10 Hz, 7 ns) tunable in the 296 to 324 nm wavelength range with a line width of 0.12 cm^{-1} . The incident laser beam is split into four beams (namely, beam1, beam2, beam3, and beam4) through the splitting system based on compensated beam-split technique (CBST). The beam splitters BS1 and BS2 are both divided into two parts made up of a half-reflective coating and an anti-reflective (AR) coating, respectively. Beam 1 and beam 2 are pump lights, and beam 3 is the probe light. The probe and the pump fields are considered to have equal amplitudes. Beam 4 is employed to determine the output direction of the DFWM signal, and it is blocked during data collection. The pump and probe lights are focused into the chamber by a quartz lens f_1 of 400 mm focal length. The DFWM signal is generated at the center of the box, and propagates along the direction of \mathbf{k}_4 , thus providing good spatial separation from the intense pump beams. The generated DFWM signal is then collimated by a quartz lens f_2 of 400 mm focal length. After being detected by a photomultiplier tube (PMT), the signal is integrated and averaged by a Boxcar gated integrator/averager, and the data are stored on a computer disk for further analysis.

3. Results and discussions

Figure 3 shows a high resolution DFWM spectrum of the transition $B^1B_1 \leftarrow X^1A_{11}$ for SO_2 , obtained with a total incident laser energy of $\approx 300 \mu\text{J}$ and a pressure of 250 Pa.

The data clearly demonstrate the spectral resolution afforded by DFWM. A comparison between the DFWM measurement and the absorption spectrum of SO_2 is also given in Fig. 3. The ratios of the DFWM line intensities differ considerably from those of the corresponding absorption spectrum. Indeed, the former is approximately

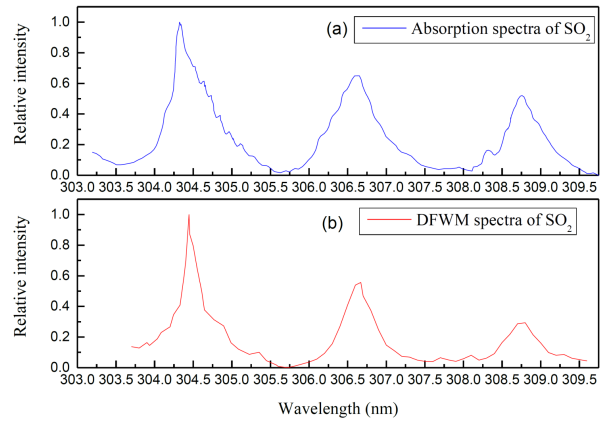


Fig. 3. Absorption spectra (a) and DFWM spectra (b) of SO_2 .

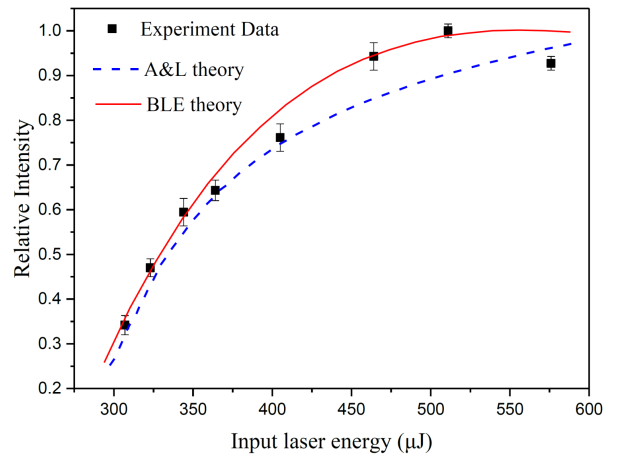


Fig. 4. The DFWM signal intensity as a function of the total input laser energy for the SO_2 .

proportional to the square of the latter, mainly as a result of the dependence of the DFWM intensity on the square of the population difference of the resonant transition.

Moreover, a difference between the line widths measured by the two techniques can also be observed. As a matter of fact, the measurement in [22] yielded a larger line width than that in the present study. The narrow line width is partly due to the elimination of the Doppler broadening achieved by the use of the phase-conjugate geometry. The results presented here demonstrate that Doppler-free, phase-conjugate DFWM offers a substantial improvement in resolution compared to Doppler-limited techniques.

The DFWM signal intensity as a function of the total input laser energy for the SO_2 is given in Fig. 4. The wavelength of the incident laser is 304.5 nm. The signal intensity rises with laser intensity and tends to saturate. While the laser energy is more than $510 \mu\text{J}$, the signal intensity shows a slight decrease as the total input laser energy increases.

The expression for the DFWM signal intensity derived by Abrams et al. was reformulated by Farrow et al. [23] in the form

$$I_{PG} = E \frac{1}{1 + (\Delta/\gamma_{12})^2} \frac{I^3/I_{\text{sat}}^2}{(1 + 4I/I_{\text{sat}})^3 \gamma_{12}^2}, \quad (1)$$

where we use the notation I_{PG} to denote the intensity of the DFWM signal originating solely from an optical absorption induced population grating. In Eq. (1) I is the laser intensity, Δ is the laser detuning and E represents a collection of constants dependent on the particular transition and experimental geometry used. I_{sat} is the saturation intensity and is given by

$$I_{\text{sat}} = \frac{\varepsilon_0 c \hbar \gamma_{12} \Gamma_0}{2|\mu_{12}|^2} \left[1 + \left(\frac{\Delta}{\gamma_{12}} \right)^2 \right], \quad (2)$$

where

$$\Gamma_0^{-1} = \frac{\gamma_1^{-1} + \gamma_2^{-1}}{2}$$

is the population decay time, and μ_{12} is the transition dipole moment.

The parameter $\gamma_{12} = \frac{\gamma_1 + \gamma_2}{2} + \gamma_{PD}$ is the coherence decay rate. γ_{PD} is given by the elastic collision frequency which derives from basic gas kinetic theory. γ_1 and γ_2 are given by

$$\gamma_1 = \frac{2\sqrt{2}\bar{c}\sigma}{kT} P_B C_{ET}, \quad (3)$$

$$\gamma_2 = \gamma_{\text{natural}} + \frac{\sqrt{2}\bar{c}}{kT} (2C_{ET}\sigma + \sigma_q) P_B, \quad (4)$$

where P_B is the partial gas pressure of the buffer gas. C_{ET} is determined by the number of degrees of freedom possessed by the buffer gas. We set $C_{ET} = 0.5$ for helium, which has 3 degrees of freedom. σ is the SO_2 /buffer gas collision cross-section, which is estimated to be $5.13 \times 10^{-19} \text{ m}^2$ [24, 25]. γ_{natural} refers to the spontaneous emission rate ($2.38 \times 10^5 \text{ s}^{-1}$ for SO_2) [24]. σ_q is quenching cross-section with the value given by [26] of $2.7 \times 10^{-20} \text{ m}^2$.

In addition to the population grating induced by optical absorption, it has been suggested that collisionally induced or thermal gratings can also generate a DFWM signal [26, 27]. The thermal grating signal can thus be expressed as

$$I_{TG} = A \left(\frac{B\sigma_q P_{\text{SO}_2} P_B}{m^{1/2}} + \frac{\sigma_B P_B^2}{m_B^{1/2}} \right) I \quad (5)$$

where the constant B accounts for the relative importance of quenching collisions to that of buffer gas collisions, m_B is the mass of the buffer gas molecule and σ_B is the collision cross-section of the buffer gas with itself ($2.1 \times 10^{-19} \text{ m}^2$ for He [26]). The parameter A in Eq. (5) is analogous to E in Eq. (1). The total observed signal can then be written as

$$I_{DFWM} = I_{PG} + I_{TG} \quad (6)$$

. The blue dashed line in Fig. 4 shows the results predicted by Eq. (6), i.e. the A&L model. In the low laser energy region, the signal intensity increases with increase

in the laser intensity, and the experimental results are consistent with the theoretical ones. On the other hand, significant deviations between the experimental results and those by the A&L model appear in the saturation region, where the results by the A&L model increase monotonically with increase in the laser intensity, which does not agree with physical reality. Indeed, from Fig. 4, it can be seen that when $I > 500 \mu\text{J}$, the signal intensity slightly decreases as the total input laser energy increases.

In order to explain this discrepancy, it is worth to point out that in the A&L theoretical model the population difference between the excited and the ground states is considered as a constant. However, as pump laser energy is increased, some particles which are pumped to the excited state will transmit to the higher rotational energy levels of the ground state. The transition process will lead to a decrease in the population difference ΔN_0 between the initial ground and excited states, which in turn results in a slight decrease of the signal intensity as the total input laser energy increases.

Moreover, the A&L model uses a perturbation theory expansion of the medium susceptibility in terms of a strong field formed by the two pump beams and a weak probe field. Indeed, in our work, the pump and the probe fields are assumed to have equal amplitudes. Both the pump and the probe beam intensities are equal or exceed the saturation level. Therefore, the A&L model does not exactly reproduce our experimental conditions.

Here, for comparison we also show theoretical results obtained by using a more sophisticated model based on BLE theory, developed by Bratfalean et al. [28]. Actually, the BLE model is used to calculate the saturation effects on spectral line shape that are relevant to simulate molecular spectra obtained by DFWM with saturating pump and probe fields.

The DFWM signal intensity is derived as

$$I_{DFWM} = \frac{\alpha_0^2 \varepsilon_0 c k^2 V^2 (1 + \delta^2) I_{\text{sat}}}{2n s^2 \pi} \times \left| \sum_{m=1}^{\infty} \frac{2^m (2m-1)! I_3^m - (1/2) I_p^m}{m! (m-1)! \bar{B}^{2m}} \times \left[-\Phi_1(f, m) + \frac{2m I_3}{(m-1)\bar{B}} \Phi_2(f, m) \right] \right|^2, \quad (7)$$

where

$$\bar{B} = (1 + \delta^2) + 2E_p^2 + E_3^2, \quad (8)$$

$$f = \frac{2E_p^2}{\bar{B}}, \quad (9)$$

The parameter $\delta = (\omega - \omega_0)T_2$ is the dimensionless detuning from the atomic resonance. T_2 is the transverse relaxation time. a_0 is the line-center small-signal-field absorption coefficient. V is the volume of the interaction region. n is the refractive index of the medium at the observation point. $\Phi_1(f, m)$ and $\Phi_2(f, m)$ are spatial integrals

$$\Phi_1(f, m) = \int_0^\pi \frac{(1 + \cos x)^m}{(1 + f \cos x)^{2m}}, \quad (10)$$

$$\Phi_2(f, m) = \int_0^\pi \frac{(1 + \cos x)^m}{(1 + f \cos x)^{2m+1}}. \quad (11)$$

Equation (7) is used to calculate the signal intensity, as a function of detuning and laser intensity respectively.

In order to calculate these theoretical spectra, a number of parameters in Eq. (7) must be specified. The value of the dipole moments is derived from the published Hönl–London factors [29]. The relative populations of the rotational levels involved is determined by the gas temperature. The value of the transverse relaxation time T_2 is not easily determined from the literature and knowledge of experimental conditions. A value of T_2 is chosen here as it is found to provide the best spectral fit.

The dependence of the DFWM signal intensity on the laser intensity as predicted by the BLE model is reported in Fig. 4 (red solid line). The deviations between the two models mainly occur in the high energy region, and the experimental trend is clearly better predicted by the BLE model than by the A&L model. This result also indicates that the BLE model more accurately predicts the DFWM signal intensity saturation effect arising from both pump and probe saturation.

The influence of molecular collisions on the production of the DFWM signal is studied. Figure 5 displays the DFWM signal as a function of the input laser energy with a buffer gas pressure of 31.5 kPa. As discussed above, the signal in Fig. 4 shows saturation. In contrast, by keeping the input laser intensities in the same range as used in Fig. 4, the DFWM signal shown in Fig. 5 is far from saturation. The DFWM saturation characteristics as shown in Figs. 4 and 5, therefore demonstrate the large variations in saturation intensity with gas pressure.

In Fig. 5, the theoretical results obtained by using the BLE model are also shown for comparison. The theoretical and experimental trends are qualitatively similar, i.e., the signal intensity increases with increasing laser intensity, and no saturation is observed. The effect of the gas pressure on the saturation laser intensity can also be understood in the framework of the BLE theory. In fact, the γ_{12} is proportional to the square of the pressure. Thus, when the gas pressure is changed by one order of magnitude, the saturation intensity I_{sat} will change, in turn, by two orders of magnitude.

In Fig. 6 the line shapes measured for different pump beam intensities and those predicted by the BLE theory (red solid lines) are shown. Based on the BLE model, when the incident beam intensity is much larger than the saturation intensity at line center, the strong beam saturates the absorbers, thereby causing decrease in the signal intensity at resonance. Therefore, for strongly saturating fields the spectrum develops the characteristic dip at line center, as shown in Fig. 6 (red solid line).

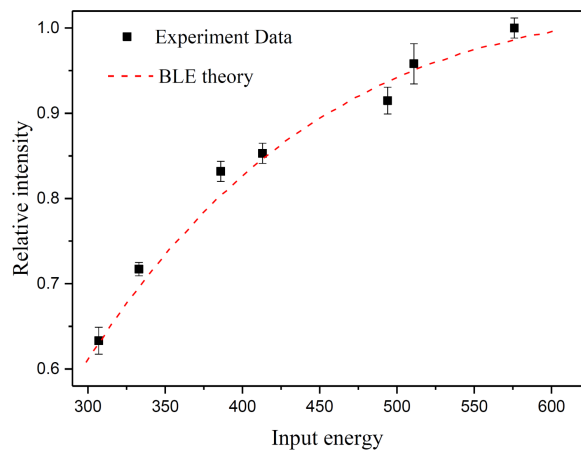


Fig. 5. The DFWM signal as a function of laser input energy with the buffer gas of helium and a pressure of 31.5 kPa.

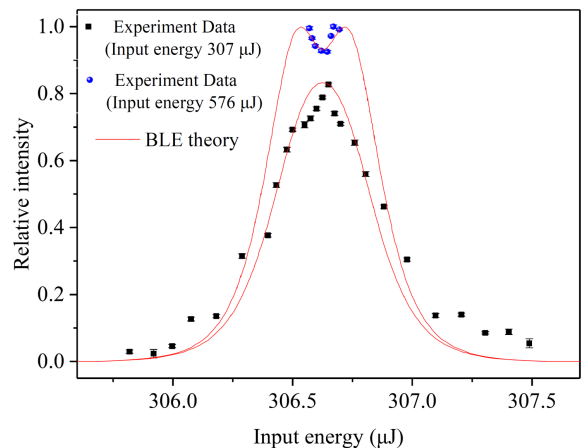


Fig. 6. The DFWM spectrum profile of SO₂ at different input laser energy.

In our experiment, when the input energy is 307 μJ , i.e., with low pump beam intensity, the maximum signal is obtained on resonance. Expectedly, as displayed in Fig. 6, a dip begins to appear at resonance when the pump beam intensity is 576 μJ . Hence, the theoretical and experimental results have similar profiles. In addition, if the incident beam is detuned, the saturation of absorbers that produces the large signal can be avoided.

4. Conclusions

An experimental investigation of the degenerate four-wave mixing spectrum of SO₂ is reported. A novel compensated beam-split technique is used to significantly improve the stability of the optical system. The DFWM spectrum of the transition $B^1B_1 \leftarrow X^1A_{11}$ for SO₂ is measured. The DFWM line intensity ratios are approximately proportional to the square of the absorption spectrum ratios. Moreover, the DFWM line widths are narrower than those of the absorption spectrum. Our result

indicates that DFWM offers a significant improvement in resolution compared to Doppler-limited techniques. DFWM saturation effects predicted by the previous theory are also experimentally verified. With the increase of the incident laser energy, a dip begins to appear at resonance in the profile.

Acknowledgments

This work is supported by the National Natural Science Foundation of China (Grant No. 11304240) and the 111 Project (Grant No. B17035).

References

- [1] M.S. Rabasovic, D. Sevic, M. Terzic, *Acta Phys. Pol. A* **116**, 570 (2009).
- [2] D. Swiech, C. Paluszkiwicz, N. Piergies, *Acta Phys. Pol. A* **133**, 286 (2018).
- [3] L. Ma, Y. Wu, W. J. Xu, S.D. Hammack, T. Lee, C.D. Carter, *Appl. Opt.* **55**, 5310 (2016).
- [4] L.R. Boeck, R. Mevel, T. Fiala, *Experim. Fluids* **57**, 1 (2016).
- [5] P. Andresen, G. Meijer, H. Schlutter et al., *Appl. Opt.* **29**, 2392 (1990).
- [6] Y. Wu, W. Xu, Q.C. Lei, *Opt. Expr.* **23**, 33408 (2015).
- [7] J. Koeser, L.G. Becker, N. Vorobiev, *Appl. Phys. B* **121**, 459 (2015).
- [8] A.J. Grant, P. Ewart, C.R. Stone, *Appl. Phys. B* **74**, 105 (2002).
- [9] T. Christopoulos, O. Tsilipakos, G. Sinatkas, E.E. Kriezis, *Phys. Rev. B* **98**, 235421 (2018).
- [10] B. Visser, M. Beck, P. Bornhauser et al., *J. Chem. Phys.* **147**, 214308 (2017).
- [11] P. Yeh, *Opt. Commun.* **51**, 195 (1984).
- [12] I. Biaggio, J.P. Partanen, B. Ai, R.J. Knize, R.W. Hellwarth, *Nature* **371**, 318 (1994).
- [13] X.L. Yin, X.M. Cheng, Y. Zhang, *Appl. Opt.* **54**, 7154 (2015).
- [14] W.B. Wang, D.Y. Chen, R.W. Fan, Y.Q. Xia, *Laser Phys.* **19**, 958 (2009).
- [15] R.L. Farrow, D.J. Rakestraw, *Science* **257**, 1894 (1992).
- [16] K. Kohse-Hinghaus, *Prog. Energy Combust. Sci.* **20**, 203 (1994).
- [17] R.L. Abrams, R.C. Lind, *Opt. Lett.* **2**, 94 (1978).
- [18] S. Williams, R.N. Zare, L.A. Rahn, *J. Chem. Phys.* **101**, 1072 (1994).
- [19] S. Williams, R.N. Zare, L.A. Rahn, *J. Chem. Phys.* **101**, 1093 (1994).
- [20] T.A. Reichart, R.P. Lucht, *J. Chem. Phys.* **111**, 10008 (1999).
- [21] D.H. Yu, J.H. Lee, J.S. Chang, *J. Opt. Soc. Am. B* **16**, 1261 (1999).
- [22] D.J. Brassington, *Appl. Opt.* **20**, 3774 (1981).
- [23] R.L. Farrow, D.J. Rakestraw, T. Dreier, *J. Opt. Soc. Am. B* **9**, 1770 (1992).
- [24] S.J. Strickler, D.B. Howell, *J. Chem. Phys.* **49**, 1947 (1968).
- [25] R.S. da Silva, M.Y. Ballester, *J. Chem. Phys.* **149**, 144309 (2018).
- [26] A.P. Smith, G. Hall, B.J. Whitaker, A.G. Astill, D.W. Neyer, P.A. Delve, *Appl. Phys. B* **60**, 11 (1995).
- [27] J.D. Garman, D. Dunn-Rankin, *SPIE Proc.* **1862**, 133 (1993).
- [28] R.T. Bratfalean, G.M. Lloyd, P. Ewart, *J. Opt. Soc. Am. B* **16**, 952 (1999).
- [29] A. Budó, *Z. Phys.* **105**, 579 (1937).